Laser Physics, 2004, 14 (6): 886-891

Monte Carlo Modeling of Polarized Light Propagation in Biological Tissues

S. V. Gangnus[1], S. J. Matcher[1], and I. V. Meglinski[2]

[1] *School of Physics, University of Exeter, Exeter, EX4 4QL, UK*

[2] *School of Engineering, Cranfield University, Cranfield, MK43 0AL, UK*

e-mail: s.j.matcher@exeter.ac.uk; i.meglinski@cranfield.ac.uk

Abstract—The application of polarization-sensitive optical coherence tomography (PS-OCT) creates new possibilities for biomedical imaging. In this work, we present a numerical simulation of the signal from a PS-OCT interferometer. We explore the possibility to retrieve information concerning the optical birefringence properties of multiple layered tissues from the depth-resolved PS-OCT interferometric signal in the presence of strong elastic light scattering. Our simulation is based on a Monte Carlo algorithm for the propagation of polarized light in a birefringent multiple scattering medium. Confocal and time-gated detection are also included. To describe the polarization state of light, we use the Jones formalism, which reduces the calculation time compared with the full Stokes–Müller formalism. To analyze the polarization state of the partially polarized backscattered light, we applied a standard method using the Stokes vector, which is derived from the Jones vector. In this work, we examined the Stokes vector variations with depth for different tissue types. The oscillations of the Stokes vector are clearly demonstrated in the case of a uniform birefringent medium. We also investigated a two-layered tissue with a different birefringence of each layer. The Stokes vector variation with depth is compared to the uniform case and used to assess the depth-sensitivity of PS-OCT. Our simulation results are also compared with published experimental results of other groups.

1. INTRODUCTION

Polarization-sensitive optical coherence tomography (PS-OCT) is a variant on an older technique, optical coherence tomography (OCT) [1, 2]. OCT is a high-resolution imaging technique offering an axial resolution of less than 20 μm (determined by the limited coherence length of the broadband source used to illuminate an interferometer). The limited coherence length of the source ensures that, at the detector, the only interferometric (coherent) signal arises from light backscattered from a well-defined depth within the tissue. This depth is given by the requirement that the sample and reference optical path lengths must be matched to within the coherence length of the source.

PS-OCT is a combination of OCT and polarization-sensitive detection [3]. A PS-OCT interferometer measures the interference fringe intensity for two orthogonal components of the electric field vector of the electromagnetic wave. It was demonstrated that a dual channel PS-OCT system, in which two detectors simultaneously record the signals from orthogonal polarization states of the emerging light, allow complete characterization of the tissue via the depth-resolved Müller matrix and Stokes parameters [4–6]. The polarization-sensitive images can provide additional information on the structure of the tissue because the polarization state of the light is changed through its interaction with biological tissues, due to both scattering and birefringence.

It has been known for over a century that collagen-rich tissues, such as tendon, cartilage, and cornea, display considerable optical birefringence [7, 8]. This is generally attributed to the high degree of physical anisotropy brought about by the directionally aligned collagen fibers, which form the extracellular matrix of the tissues. The molecular packing structure of the collagen fibers is such that the index of refraction is higher along the length of the fiber than along the cross section, leading to linear birefringence.

The change of state of the polarization at the scattering was considered in recent papers [9, 10], where Monte Carlo (MC) simulation for a multiple scattering process in a turbid medium was used and the experimental results were presented. In [11], the results of simulation based on the Stokes–Müller formalism were presented. This simulation was based on an MC algorithm combining the birefringent and multiple scattering of the medium for backscattered light.

In this work, we present a Monte Carlo algorithm that combines a rigorous treatment of the change in the polarization of light due to both scattering and birefringence using the more effective/fast Jones formalism with confocal- and coherence-gated detection.

2. BASIC MONTE CARLO TECHNIQUE

The principles of the MC method have been widely described elsewhere. This method is based on the random simulation of a large number of possible trajectories of photons as they travel through a highly scattering medium. The simulation consists of a sequential random walk of photon packets between scattering events from the site of photon injection into the

medium to the site where the photon leaves the medium. Total internal reflection on the medium boundary is taken into account as suggested in [12]. OCT generally entails both spatial and temporal filtering of the backscattered signal. To implement confocal spatial filtering, we followed a scheme developed early [13] and illustrated in Fig. 1. Objective lens L_1 collects an exiting photon packet, which is refocused onto a pinhole of diameter d by lens L_2. By recording the position (x_m, y_m) and exit angle of a photon packet as it leaves the medium, one can easily calculate the position (x_d, y_d) where the photon packet traverses the detection plane using

$$\begin{aligned} x_d &= (f-h)\alpha_x - x_m, \\ y_d &= (f-h)\alpha_y - y_m. \end{aligned} \tag{1}$$

Here, f is the focal length of L_1 and L_2, h is the distance of L_1 from the medium surface, and α_x is the angle between the photon exit trajectory (projected onto the x–z plane) and the normal to the medium surface $\hat{z}$ (projected onto the α_y plane).

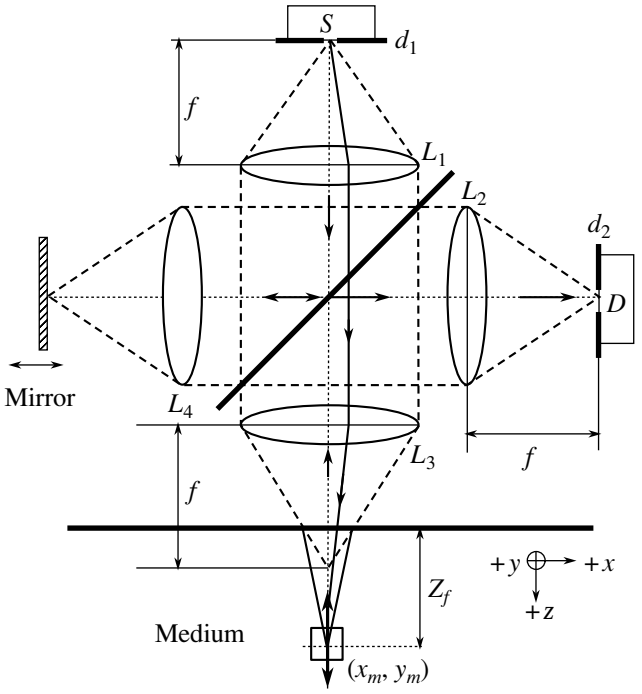

Fig. 1. Schematic of the confocal/OCT detection: L_1, L_2, L_3, L_4 are the short focus lenses (f = 8 mm) producing pairs of narrow aperture collimators; d_1 and d_2 are diaphragms 10 μm in diameter; Z_f is the focal point depth within the medium; S is the laser source (P = 0.2 μW, λ = 1025 nm, $l_c \approx 20$ μm); D is the detector of optical radiation; and n_0 and n_1 are the refractive indices of external and modeling media, respectively. The line with arrows shows an example of detected signal: source–medium–pinhole detector.

3. JONES AND STOKES–MÜLLER FORMALISMS

The transmission of polarized light through a scattering and birefringent medium can be treated with various methods. This work presents a Monte Carlo simulation for polarized light using the matrix formalism developed by Jones [14, 15]. This formalism describes the polarized light as a two-element matrix, the Jones vector:

$$J = \begin{bmatrix} E_s \\ E_p \end{bmatrix}. \tag{2}$$

Here, E_s, E_p are two orthogonal components of the electric field vector of the electromagnetic wave. The transmission of this wave through a polarizing medium is described by a 2×2 matrix:

$$J_{out} = M \bullet J_{in} = \begin{bmatrix} m_{11} & m_{12} \\ m_{21} & m_{22} \end{bmatrix} \bullet J_{in}, \tag{3}$$

where J_{in} and J_{out} are the Jones vectors before and after the polarizing element and M is the Jones matrix within general complex elements.

The original matrix formalism developed by Jones is restricted to describing the propagation of polarized light through a birefringent medium only at normal incidence. The extended Jones matrix method was introduced to overcome this limitation and describe nonnormal propagation [16, 17]. The method can thus be used to describe the transmission of off-axis light through a multilayer birefringent medium.

An alternative treatment of polarized light propagation is based on the Stokes–Müller formalism, where the state of the polarization is described by a Stokes vector

$$S = \begin{bmatrix} S_0 \\ S_1 \\ S_2 \\ S_3 \end{bmatrix} = \begin{bmatrix} E_s^2 + E_p^2 \\ E_s^2 - E_p^2 \\ E_s^* E_p + E_s E_p^* \\ i(E_s^* E_p - E_s E_p^*) \end{bmatrix} \tag{4}$$

and transmission through a polarizing element, by a 4×4 matrix

$$S_{out} = LS_{in} = \begin{bmatrix} l_{11} & l_{12} & l_{13} & l_{14} \\ l_{21} & l_{22} & l_{23} & l_{24} \\ l_{31} & l_{32} & l_{33} & l_{34} \\ l_{41} & l_{42} & l_{43} & l_{44} \end{bmatrix} S_{in}, \tag{5}$$

where the matrix L is the Müller matrix with 16 real elements.

If polarized light propagates through several polarizing elements, the resulting Jones or Müller matrices are given by the product of each element. All 16 elements of the Müller matrix can be found from four complex elements (that is, eight real numbers) of the Jones matrix, and the Stokes vector is derived from the Jones vector:

$$\begin{aligned}
l_{11} &= (m_{22}^2 + m_{11}^2 + m_{12}^2 + m_{21}^2)/2,\\
l_{12} &= (m_{11}^2 - m_{22}^2 + m_{21}^2 - m_{12}^2)/2,\\
l_{13} &= \mathrm{Re}\{m_{11}m_{12}^* + m_{22}m_{21}^*\},\\
l_{14} &= \mathrm{Im}\{m_{11}m_{12}^* - m_{22}m_{21}^*\},\\
l_{21} &= (m_{11}^2 - m_{22}^2 - m_{21}^2 + m_{12}^2)/2,\\
l_{22} &= (m_{11}^2 + m_{22}^2 - m_{21}^2 - m_{12}^2)/2,\\
l_{23} &= \mathrm{Re}\{m_{11}m_{12}^* - m_{22}m_{21}^*\},\\
l_{24} &= \mathrm{Im}\{m_{11}m_{12}^* + m_{22}m_{21}^*\},\\
l_{31} &= \mathrm{Re}\{m_{11}m_{21}^* + m_{22}m_{12}^*\},\\
l_{32} &= \mathrm{Re}\{m_{11}m_{21}^* - m_{22}m_{12}^*\},\\
l_{33} &= \mathrm{Re}\{m_{22}m_{11}^* + m_{12}m_{21}^*\},\\
l_{34} &= \mathrm{Im}\{m_{11}m_{22}^* + m_{21}m_{12}^*\},\\
l_{41} &= \mathrm{Im}\{m_{11}^*m_{21} + m_{12}^*m_{22}\},\\
l_{42} &= \mathrm{Im}\{m_{11}^*m_{21} - m_{12}^*m_{22}\},\\
l_{43} &= \mathrm{Im}\{m_{22}m_{11}^* - m_{12}m_{21}^*\},\\
l_{44} &= \mathrm{Re}\{m_{22}m_{11}^* - m_{12}m_{21}^*\}.
\end{aligned} \tag{6}$$

Therefore, Jones formalism is simpler and easier to use in calculation than Stokes–Müller formalism and is preferable for the description of polarized light in a Monte Carlo simulation.

4. MONTE CARLO ALGORITHM FOR A UNIAXIAL BIREFRINGENT TURBID MEDIUM

The proposed Monte Carlo simulation consists of two steps. First, a large number of photon histories are generated and stored on hard disk. Then, the transformation of the Jones vector is calculated to describe the polarization state of each emerging photon packet after N scattering interactions as

$$J_{\mathrm{out}} = \left[\prod_{j=1}^{N} R(-\psi_j)P(k_0, k_{ej}, l_j)R(\psi_j)S(\theta'_j)R(\varphi'_j)\right]J_{\mathrm{in}}, \tag{7}$$

$$R(\psi) = \begin{bmatrix}\cos\psi & -\sin\psi\\ \sin\psi & \cos\psi\end{bmatrix}, \tag{8a}$$

$$R(\varphi') = \begin{bmatrix}\cos\varphi' & -\sin\varphi'\\ \sin\varphi' & \cos\varphi'\end{bmatrix}, \tag{8b}$$

$$P(k_0, k_e, l) = \begin{bmatrix}\exp(-ik_o l) & 0\\ 0 & \exp(-ik_e l)\end{bmatrix}, \tag{9}$$

$$S(\theta') = \begin{bmatrix}S_2(\theta') & S_3(\theta')\\ S_4(\theta') & S_1(\theta')\end{bmatrix}. \tag{10}$$

Here, J_{in} and J_{out} represent the Jones vectors of the incident and the detected photon packets, respectively; $R(\psi)$ is the rotation matrix; ψ defines the angle between the fast axes of the birefringent medium and the component E_s of the electric field of an electromagnetic wave; $P(k_o, k_e, l)$ is the propagation matrix describing phase retardation between the ordinary and extraordinary rays with k_o and k_e wave numbers, respectively; l is the distance traversed by the photon within the birefringent medium; $R(\varphi')$ is the rotation matrix, whose angle φ' describes the change of the azimuth angle of the photon trajectory relative to the old direction due to a scattering event; and $S(\theta')$ is the matrix for each single scattering event derived from Mie theory, where θ' is the polar scattering angle. We used a published source code from [18] to calculate this scattering matrix for homogeneous spherical scatterers.

The wave number for the extraordinary wave can be derived using the expression for the normal surface of the birefringent medium [17] given by

$$\frac{k_{ea}^2 + k_{eb}^2}{n_e^2} + \frac{k_{ec}^2}{n_o^2} = \left(\frac{\omega}{c}\right)^2. \tag{11}$$

Here, n_o and n_e are the ordinary and the extraordinary indices of refraction, respectively; ω is the angular frequency of the wave; c is the speed of light in vacuum; and k_{ea}, k_{eb}, and k_{ec} are the wave-vector components of the extraordinary wave in the principal coordinate system defined as

$$k_{ea} = (\alpha\cos\varphi_c + \beta\sin\varphi_c)\cos\theta_c - k_e\sin\theta_c, \tag{12}$$

$$k_{eb} = -\alpha\sin\varphi_c + \beta\cos\varphi_c, \tag{13}$$

$$k_{ec} = (\alpha\cos\varphi_c + \beta\sin\varphi_c)\sin\theta_c + k_e\cos\theta_c, \tag{14}$$

where the indices a, b, and c are referred to the principal coordinate system (a, b, c) and α, β, and k_e are the projections of the wave vector on the axes of the local coordinate system of a photon packet. The vector c is in line with the orientation of the optic axis of the birefringent medium. The vectors a and b are perpendicular to c and

Parameters used in the simulation

D	Pinhole diameter	10 μm
f	Focal length	8 mm
NA	Numerical aperture	0.25
h	Lens height over medium	7.95 mm
λ	Wavelength	1300 nm
μ_s	Scattering coefficient	25 mm^{-1}
μ_a	Absorption coefficient	0.015 mm^{-1}
n	Refractive index of medium	1.47
Δn	Birefringence	0.01
n_{sca}	Refractive index of scattering particle	1.55
RAD	Diameter of scattering particle	1000 nm

each other. Substituting Eqs. (12)–(14) into Eq. (11), we obtain

$$uk_e^2 - vk_e + w = 0, \tag{15}$$

where

$$u = \frac{\sin^2\theta_c}{n_e^2} + \frac{\cos^2\theta_c}{n_o^2}, \tag{16}$$

$$v = k_d \sin(2\theta_c)\left(\frac{1}{n_e^2} - \frac{1}{n_o^2}\right), \tag{17}$$

$$w = \frac{k_d^2\cos^2\theta_c + k_{eb}^2}{n_e^2} + \frac{k_d^2\sin^2\theta_c}{n_o^2} - \left(\frac{\omega}{c}\right)^2, \tag{18}$$

with

$$k_d = \alpha\cos\varphi_c + \beta\sin\varphi_c. \tag{19}$$

Solving Eq. (15), we obtain the wave number of the extraordinary wave:

$$k_e = \lfloor v + (v^2 - 4uw)^{1/2} \rfloor/(2u). \tag{20}$$

The wave number of the ordinary wave is given by

$$k_o = [(n_o\omega/c)^2 - \alpha^2 - \beta^2]^{1/2}. \tag{21}$$

5. RESULTS

In our simulation, we launched 10^9 photons, of which 10^6 were detected. These 10^6 traces were stored on hard disk. The simulation parameters are listed in the table. The basic Monte Carlo code to generate these parameters required about 400 h of calculation on a 1 GHz Athlon processor. This ASCII data file took

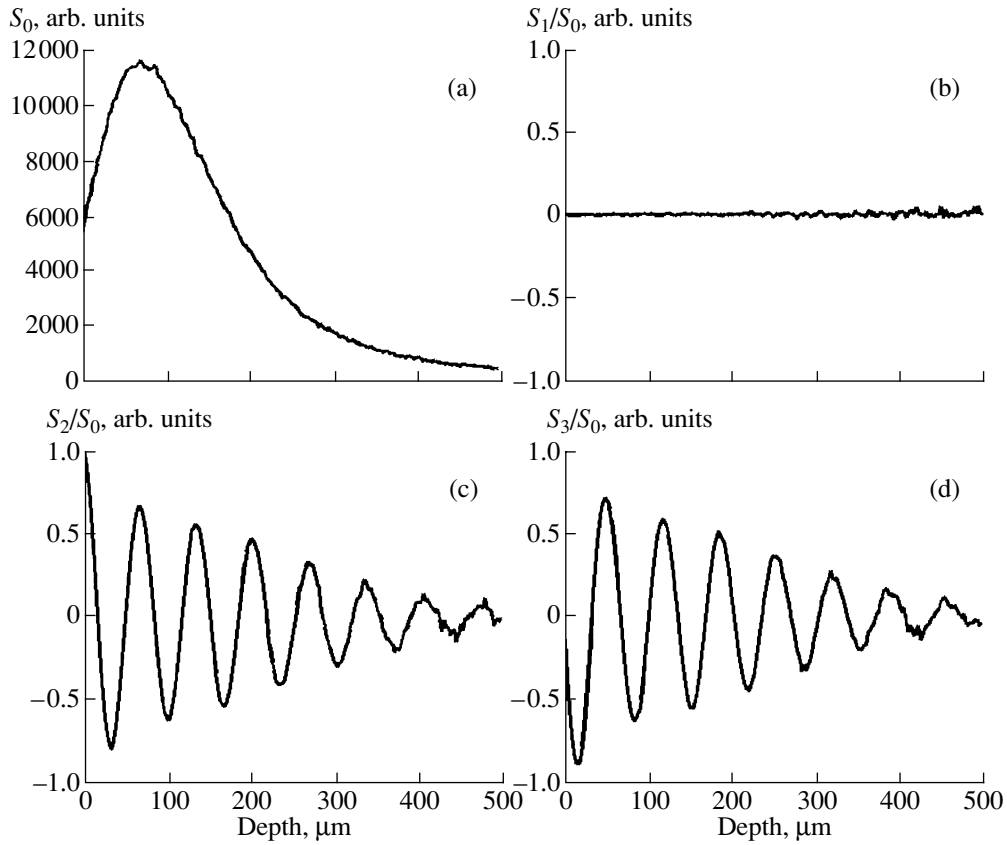

Fig. 2. Stokes vector for homogeneous tissue linearly polarized at +45° incident light: (a) S_0 parameter, (b–d) parameters S_1, S_2, and S_3.

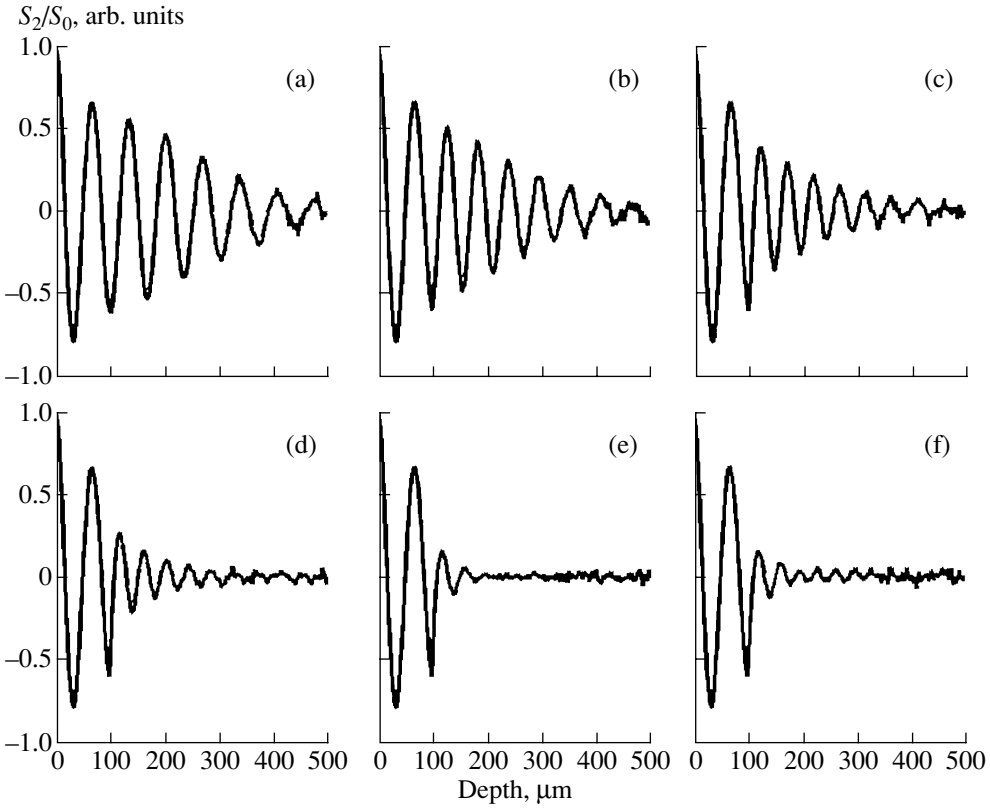

Fig. 3. Normalized depth-resolved Stokes parameter S_2 of a two-layer tissue (boundary at depth 100 μm). The fast axis orientation is identical for both layers, but the birefringence Δn is greater in the deeper layer by Δn_{21}, where Δn_{21} = (a) 0, (b) 0.002, (c) 0.004, (d) 0.006, (e) 0.008, and (f) 0.01.

500 Mb of disk space. OCT detection is realized by selecting photon packets according to their transit time in the medium. The calculation of the polarization state of these detected photons required 10 min.

To analyze the polarization state of the partially polarized backscattered light, we applied a standard method using the Stokes vector $S = (S_0, S_1, S_2, S_3)^T$, which is derived from the Jones vector (see Eq. (3)). The element S_0 describes the overall intensity of the backscattered light. The element S_1 corresponds to vertical or horizontal linearly polarized light. The element S_2 describes light linearly polarized at 45° to the horizontal/vertical. The last element S_3 describes circularly polarized light. Figure 2 shows the Stokes vector parameters of backscattered photons, with a range of the path length from 0 to 1000 μm (presented here as the penetration depth in the range 0–500 μm). The incident light is assumed to be linearly polarized at +45°.

The oscillations of the Stokes vector are clearly seen in the case of a uniform birefringent medium. The birefringence Δn can readily be calculated from the oscillation period of the S_2 or S_3 parameters. The oscillation period d equals approximately 65 μm (see Fig. 2) and is related to Δn via

$$2\pi = \frac{2\pi}{\lambda}\Delta n(2d). \qquad (22)$$

Therefore, the value of d corresponds to a birefringence $\Delta n = 0.01$, which matches the value of birefringence originally specified in the table. This gives us confidence that the simulation code is working correctly. The results of the simulation also show qualitative agreement with recently reported experimental results [19], where the oscillations of Stokes parameters were observed for rodent muscle.

We also investigated a two-layered tissue with different birefringence properties in each layer. Figure 3 shows the normalized depth-resolved Stokes parameter S_2 of a two-layered tissue. The depth of the boundary is 100 μm. This figure demonstrates how the depth-resolved Stokes parameters depended on the difference in the birefringence of the layers $\Delta n_{21} = \Delta n_2 - \Delta n_1$, where Δn_1 and Δn_2 are the birefringence between the first and second layers. Figure 3a corresponds to identical birefringence in both layers and shows only the effect of depolarization with depth. The other plots (Figs. 3b–3f) are made for different steadily increasing

values of the birefringence mismatches between layers Δn_{21}. It is seen that the increase of Δn_{21} leads to a stronger decay of depth-resolved Stokes parameters with depth, i.e., a stronger depolarization of backscattered light. This result is interesting, and we are currently working to understand this effect.

6. CONCLUSIONS

We have developed a Monte Carlo model for polarized light propagation in a birefringent multiple scattering multilayered medium. By including confocal and time-gated detection, the code can be used to model the signal from a PS-OCT interferometer. This makes it possible to assess the depth-sensitivity of PS-OCT and model different types of tissues with more complicated structure.

We have investigated one- and two-layer birefringent turbid tissues. The Stokes vector variations with depth were simulated. The oscillations of the Stokes vector were clearly observed in the case of the birefringent medium. This result shows qualitative agreement with published experimental results of other groups. The effects of scattering-induced depolarization are clearly shown and demonstrate that the "single backscatter" model does not describe PS-OCT well. In a homogeneous medium, with optical transport properties similar to real tissue, the amplitude of the oscillations in the Stokes parameters decreases to 10% of its initial value at a depth of approximately 500 μm. The influence of the spatial nonuniformity of the medium birefringence has also been considered. It has been found that the effect of depolarization for a nonuniform birefringent medium is stronger than that for uniform birefringent tissue. This question will receive further consideration in later work.

ACKNOWLEDGMENTS

The authors would like to acknowledge the support of the Medical Research Council, grant no. G0001108. S.V. Gangnus gratefully acknowledges support via the Royal Society/NATO Postdoctoral Research Fellowship scheme.

REFERENCES

1. D. Huang, E. A. Swanson, C. P. Lin, *et al.*, Science **254**, 1178 (1991).
2. E. A. Swanson, J. R. Izatt, M. R. Hee, *et al.*, Opt. Lett. **18**, 1864 (1993).
3. M. R. Hee, D. Huang, E. A. Swanson, and J. G. Fujimoto, J. Opt. Soc. Am. B **9**, 903 (1992).
4. J. F. de Boer, T. E. Milner, M. J. C. van Gemert, and J. S. Nelson, Opt. Lett. **22**, 934 (1997).
5. K. Schoenenberger, B. W. Colston, D. J. Maitland, *et al.*, Appl. Opt. **37**, 6026 (1998).
6. X.-J. Wang, T. E. Milner, J. F. de Boer, *et al.*, Appl. Opt. **38**, 2092 (1999).
7. D. J. Donohue, B. J. Stoynov, R. L. McCally, and R. A. Farrell, J. Opt. Soc. Am. A **12**, 1425 (1995).
8. V. F. Izotova, I. L. Maksimova, I. S. Nefedov, and S. V. Romanov, Appl. Opt. **36,** 164 (1997).
9. S. Bartel and A. H. Hielscher, Appl. Opt. **31**, 1580 (2000).
10. A. S. Martinetz and R. Maynard, *Photonic Band Gaps and Localization* (Plenum, New York, 1993).
11. X. Wang and L. V. Wang, Opt. Express **9**, 254 (2001).
12. D. Y. Churmakov, I. V. Meglinski, and D. A. Greenhalgh, Phys. Med. Biol. **47**, 4271 (2002).
13. I. V. Meglinski, A. N. Bashkatov, E. A. Genina, *et al.*, Quantum Electron. **32**, 875 (2002).
14. R. C. Jones, J. Opt. Soc. Am. **31**, 488 (1941).
15. H. Hurwitz and R. C. Jones, J. Opt. Soc. Am. **31**, 493 (1941).
16. P. Yeh, J. Opt. Soc. Am. **72**, 507 (1982).
17. C. Gu and P. Yeh, J. Opt. Soc. Am. **10**, 966 (1993).
18. C. F. Bohren and D. R. Huffman, *Absorption and Scattering of Light by Small Particles* (Wiley, New York, 1998; Mir, Moscow, 1986).
19. J. F. de Boer, T. E. Milner, and J. S. Nelson, Opt. Lett. **24**, 300 (1999).